Signature of tropical fires in the diurnal cycle of tropospheric CO as seen from Metop-A/IASI

T. Thonat, C. Crevoisier, N. A. Scott, A. Chédin, R. Armante, L. Crépeau

Atmos. Chem. Phys., 15, 13041–13057, 2015
www.atmos-chem-phys.net/15/13041/2015/
doi:10.5194/acp-15-13041-2015

Atmospheric Chemistry and Physics Open Access EGU

Signature of tropical fires in the diurnal cycle of tropospheric CO as seen from Metop-A/IASI

T. Thonat, C. Crevoisier, N. A. Scott, A. Chédin, R. Armante, and L. Crépeau

Laboratoire de Météorologie Dynamique, CNRS, IPSL, École Polytechnique, Palaiseau, France

Correspondence to: T. Thonat (thibaud.thonat@lmd.polytechnique.fr)

Received: 23 July 2014 – Published in Atmos. Chem. Phys. Discuss.: 17 October 2014
Revised: 18 October 2015 – Accepted: 11 November 2015 – Published: 25 November 2015

Abstract. Five years (July 2007 to June 2012) of CO tropospheric columns derived from the hyperspectral Infrared Atmospheric Sounding Interferometer (IASI) on-board Metop-A are used to study the impact of fires on the concentrations of CO in the troposphere. Following Chédin et al. (2005, 2008), who found a quantitative relation between the daily tropospheric excess of CO_2 and fire emissions, we show that tropospheric CO also displays a diurnal signal with a seasonality that agrees well with the seasonal evolution of fires given by Global Fire Emission Database version 3 (GFED3.1) and Global Fire Assimilation System version 1 (GFAS1.0) emissions and Moderate Resolution Imaging Spectroradiometer (MODIS) Collection 5 burned area product. Unlike day- or night-time CO fields, which mix local emissions with nearby emissions transported to the region of study, the day–night difference of CO allows to highlight the CO signal due to local fire emissions. A linear relationship between CO fire emissions from the GFED3.1 and GFAS1.0 inventories and the diurnal difference of IASI CO was found over various regions in the tropics, with a better agreement with GFAS1.0 (correlation coefficient of $R^2 \sim 0.7$) than GFED3.1 ($R^2 \sim 0.6$). Based on the specificity of the two main phases of the combustion (flaming vs. smoldering) and on the vertical sensitivity of the sounder to CO, the following mechanism is proposed to explain such a CO diurnal signal: at night, after the passing of IASI at 21:30 local time (LT), a large amount of CO emissions from the smoldering phase is trapped in the boundary layer before being uplifted the next morning by natural and pyroconvection up to the free troposphere, where it is seen by IASI at 09:30 LT. The results presented here highlight the need to take into account the specificity of both the flaming and smoldering phases of fire emissions in order to fully take advantage of CO observations.

1 Introduction

Biomass burning plays an important and singular role in the global carbon cycle, with a combination of human and natural drivers. Fire emissions are a major source of carbon in the atmosphere, particularly in the forms of carbon dioxide (CO_2) and carbon monoxide (CO). Global emissions can vary significantly from year to year. According to van der Werf et al. (2010), in the 1997–2009 period, they have varied between 1.5 and 3 PgC yr^{-1}. Global emission estimates can also differ from one inventory to another: for the year 2000 for example, Ito and Penner (2004) evaluated them at 1.4 PgC while Schultz et al. (2008) made the estimate of 2.3 PgC. On average between 1997 and 2009, the emissions are up to 2 PgC yr^{-1} (van der Werf et al., 2010). This represents the equivalent of about one third of the total anthropogenic emissions related to fossil fuel combustion and cement production (IPCC, 2007). These global emissions are not in total a net contribution to the atmosphere since the carbon released is partly recaptured by photosynthesis during the consecutive growth of plants. Nonetheless, they are important enough to be the main factor driving the variability of the CO_2 growth rate (Langenfelds et al., 2002). The influence of fires on climate occurs in several ways: they globally reinforce climate change (Bowman et al., 2009); they globally reduce surface albedo by producing soot; they release various chemical compounds which can reach the free troposphere (Lavoué, 2000) and then be transported around the globe (e.g. Freitas et al., 2006; Guan et al., 2008) and af-

fect the atmospheric chemistry; aerosols emitted by fires can modify cloud coverage and precipitation patterns (Andreae, 1991; Andreae et al., 2004). However, despite their magnitude, current estimates of fire emissions of gases and aerosols still remain affected by large uncertainties.

Throughout the years, several fire emission inventories have been built based on various approaches (e.g. Hoelzemann et al., 2004; Jain et al., 2006; Lehsten et al., 2009; van der Werf et al., 2010). Most of them rely on the following equation to compute fire emissions:

$$M = A \times B \times e \times \mathrm{EF}, \quad (1)$$

where M (g) is the product of the burned areas A (m^2), the biomass density B ($g\,m^{-2}$), the combustion efficiency e ($g\,g^{-1}$) and the emission factor (EF) which depends on the studied gas (Seiler and Crutzen, 1980). A is determined from observations from space, B and e are generally given by a biogeochemical model and EF is calculated empirically, mainly based on field measurements. However, large uncertainties affect each term of this equation, meaning that these inventories alone are not sufficient to determine all the characteristics of fires and their emissions.

More recently, the GFAS1.0 (Global Fire Assimilation System) emissions inventory (Kaiser et al., 2012) was built and does not rely on Eq. (1). It is based on the relation between the fire radiative power (FRP) and fire emissions themselves. All fuels release approximately the same quantity of energy per mass unit. Assuming that the fire radiative energy (FRE) is proportional to the total energy released by a fire, it is possible to estimate the quantity of burned biomass. Wooster et al. (2005) have shown that there was a linear relation between the FRE and the mass of burned fuels and found a universal conversion factor. Estimates relying on this method are not dependent on the terms A, B and e of Eq. (1). However, uncertainties remain in the measure of the FRP from polar satellites, in the determination of the emission factors and in the estimation of the conversion factor (e.g. Freeborn et al., 2008) and its dependence on the vegetation type.

A more direct measure from space, which is by nature global and continuous, of biomass burning carbon emissions themselves, and more particularly of CO_2 and CO, could in principle allow us to avoid the difficulties encountered in the bottom-up approach and provide a necessary complement to the inventories. Several studies have relied on CO observations from space, mostly from thermal infrared sounders, to quantify fire emissions. Indeed, since fires emit large amounts of CO into the atmosphere far above its background level, CO is known as a good proxy of fire emissions. For example, continuous CO measurements, in particular with the Measurements Of Pollution In The Troposphere (MOPITT) instrument, have been compared to chemistry-transport simulations based on fire emission inventories (e.g. Turquety et al., 2007; Yurganov et al., 2008). Atmospheric Infrared Sounder (AIRS) was the first instrument to provide daily global measurements of CO, highlighting the large-scale transport of fire emissions (McMillan et al., 2005, 2008). Observations from the more recent IASI (Infrared Atmospheric Sounding Interferometer) instrument (Hilton et al., 2012) have also been used for example to study extreme fire events in Russia in 2010 (Yurganov et al., 2011) or in Greece in 2007, where GFED2 (Global Fire Emission Database) emissions were shown to be undervalued (Turquety et al., 2009). CO is a good indicator of fire activity, but it only represents a small fraction of the emissions, which is mostly representative of the smoldering phase of the combustion (Lobert and Warnatz, 1993). Therefore CO_2, which represents the majority of the emissions and is mostly representative of the flaming phase of the combustion, has also been studied in relation with fire activity despite the difficulty of both retrieving CO_2 from space and capturing the "fire signal" in its tropospheric concentration.

An approach developed by Chédin et al. (2005, 2008) allows the isolatation of CO_2 fire emissions from space by calculating the difference between CO_2 retrieved by night and CO_2 retrieved by day that results from the diurnal cycle of fires (Giglio, 2007). This difference is calculated from the observations of TIROS-N Operational Vertical Sounder (TOVS) on-board NOAA10 and is called daily tropospheric excess (DTE). It can reach several ppmv (parts per million by volume) over regions affected by fires. The seasonal and interannual variabilities of the DTE are in agreement with burned areas and fire emissions, showing that there is an excess of CO_2 in the troposphere above burned areas at 19:30 LT, a few hours after the peak of fire activity, compared to the CO_2 level at 07:30. The DTE was shown to be quantitatively related to CO_2 fire emissions in the tropics. The mechanism explaining the observation of such a signal is as follows: (i) in the afternoon, during the period of high fire activity, large quantities of CO_2 are emitted into the free troposphere; (ii) CO_2 accumulates under the tropopause and is seen by the satellite at 19:30; (iii) CO_2 is then diluted by large-scale transport during the 12 h preceding the next pass of the satellite, at 07:30, before fires start again. This result was theoretically confirmed with a pyro-thermal plume model (Rio et al., 2010).

As Metop passing times are 09:30/21:30, i.e. before and after the maximum of the diurnal cycle of fires, IASI is well suited to complete the study of the diurnal cycle of fire emissions initiated with TOVS. The main difficulty of the DTE remains in the retrieval of CO_2 and the weakness of the CO_2 fire signal. On the contrary, the impact of fires on the concentration of CO can be more than 100 % of its background level (e.g. Turquety et al., 2009), providing a clearer signal with respect to fires. For these reasons, our study focuses on CO and particularly on its diurnal variation in relation to fire activity. Our study focuses on tropical biomass burning regions in the years 2007–2012. Section 2 describes the data and the method used to retrieve CO from the IASI observations. Section 3 presents the IASI retrievals, by day and

by night, in comparison with fire activity. We first focus on southern Africa, where fire emissions are particularly strong, and then on various regions in the tropics. Section 4 is a discussion of why the diurnal difference of CO is in better agreement with fire activity than the daytime or night-time concentrations. Section 5 concludes this study.

2 Data and method

2.1 IASI

The Infrared Atmospheric Sounding Interferometer is a polar-orbiting nadir-viewing instrument that measures infrared radiation emitted from the Earth. IASI is a high-resolution Fourier transform spectrometer based on a Michelson Interferometer, which provides 8461 spectral samples, ranging from 645 to 2760 cm^{-1} (15.5 and 3.6 µm), with a spectral sampling of 0.25 cm^{-1} and a spectral resolution of 0.5 cm^{-1} after apodization ("Level 1c" spectra). IASI cross-track scanning is of 2200 km at the surface, allowing global coverage twice a day. The instantaneous field of view is sampled by 2×2 circular pixels whose ground resolution is 12 km at nadir. IASI was developed by the Centre National d'Etudes Spatiales (CNES) in collaboration with the European Organisation for the Exploitation of Meteorological Satellites (EUMETSAT); it was launched in October 2006 on-board the polar-orbiting Meteorological Operational Platform (Metop-A) and has been operational since July 2007. In this study, use is made of the Level 1c data (available from the Ether Centre for Atmospheric Chemistry Products and Services website: http://ether.ipsl.jussieu.fr/, via EUMETCast).

2.2 Retrieval method

The retrieval scheme is based on the double difference approach described in Thonat et al. (2012), which takes advantage of the high spectral resolution of IASI. It relies on the idea of using a difference in brightness temperature (BT) between two channels having the same sensitivities to every atmospheric and surface variable but CO. This difference is thus only sensitive to CO variations and cancels out the signals coming from interfering variables (surface temperature and emissivity, temperature, water vapour and nitrous oxide). In order to interpret this BT difference in terms of CO, we use the difference between the BT simulated by the 4A (Automatized Atmospheric Absorption Atlas) (Scott and Chédin, 1981; http://ara.abct.lmd.polytechnique.fr/) radiative transfer model and the observed BT. The double difference then provides the amount of CO in the troposphere which is in excess (or deficit) in comparison with the a priori CO profile used as input in 4A.

For the simulated BT, use is made of the European Centre for Medium-Range Weather Forecasts (ECMWF) ERA-Interim Reanalyses as atmospheric data input to 4A. These are profiles of temperature, water vapour and ozone characterized by a 6 h time resolution and a $0.75° \times 0.75°$ spacial resolution, colocalized in time and space to IASI clear-sky fields of view and inter-/extrapolated on the 4A pressure levels. The surface temperature is estimated directly from one IASI channel (at 2501.75 cm^{-1}) to avoid the lag between the closest reanalyses and the IASI passing. The same a priori CO profile is used for every simulation. For observed BT, clouds and aerosols are detected with several threshold tests based on IASI and AMSU observations (Crevoisier et al., 2003; Pierangelo et al., 2004).

The retrieved CO column is representative of the mid-troposphere, with a maximum sensitivity at about 450 hPa, and half a maximum between about 200 and 750 hPa, depending on the difference between surface temperature and above air temperature: the higher this difference, which is defined as the "thermal contrast", the higher the sensitivity to CO in the lower layers of the troposphere. The retrieval method also gives access to the precision, which is about 2.5 ppbv.

CO retrievals from IASI have been compared with the CARIBIC (Civil Aircraft for the Regular Investigation of the Atmosphere Based on an Instrument Container) (Brenninkmeijer et al., 2007) aircraft measurements. The difference between CARIBIC and IASI CO is on average 3.6 ppbv, with a standard deviation of 13.0 ppbv. This agreement is also found above deserts and mountainous areas, highlighting that the retrievals are not impacted by surface characteristics (Thonat et al., 2012).

3 The diurnal variation of IASI tropospheric CO

3.1 IASI day- and night-time CO over the tropics

Five whole years of clear-sky observations from the IASI hyperspectral infrared sounder between July 2007 and June 2012 have been interpreted in terms of tropospheric CO column, in the tropics (30° N to 30° S), by day and night (09:30/21:30 LT). Maps of monthly means of CO in the troposphere are plotted in Fig. 1 on a $0.75° \times 0.75°$ grid, for January, April, July and October 2008, over land and over sea. Blank areas denote an absence of retrievals due to persistent cloudiness or aerosols. According to Fig. 1, the distribution and the seasonality of CO retrieved by day and night are similar, though with lower maximum values in the night-time.

Highest CO concentrations are localized above continents, in the Northern Hemisphere (NH) during the boreal winter and in the Southern Hemisphere (SH) during the austral winter. These extreme values, which concern primarily Africa and South America, stem from important biomass burning events in the local dry season (Duncan et al., 2003). Fires are not the only source of CO in the tropics; for example high CO values are seen in China outside of the fire season, caused

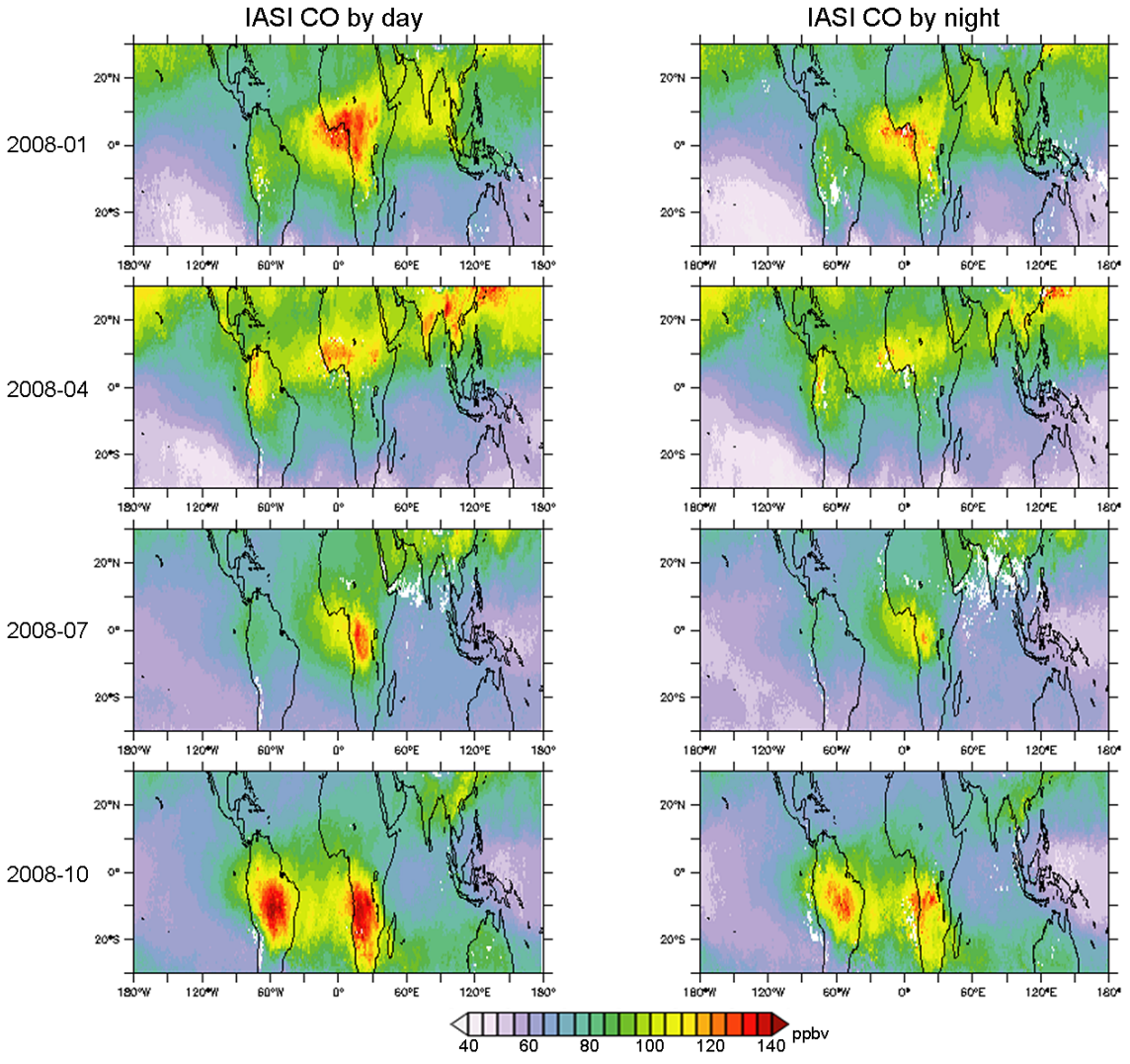

Figure 1. Monthly means of the integrated content of CO from IASI (ppbv), by day (09:30 LT) (left) and by night (21:30 LT) (right), in January, April, July and October 2008 in the tropics.

by a continuous pollution coming from fossil fuel combustion (industry, transport) (Buchwitz et al., 2007; Streets et al., 2006).

The repartition of CO seen in Fig. 1 is also influenced by the seasonal variation of the OH radical, the main sink of CO (Holloway, 2000). During the boreal winter, OH concentrations are low in the north and high in the south (Spivakovsky et al., 1990), allowing CO emitted by fires and human activities to accumulate in the NH (Duncan et al., 2007). The opposite happens during the winter in the SH, where the anthropogenic emissions play a less important role.

High CO concentrations are also seen over sea because of the transport from continental sources. Indeed, in the mid-troposphere, where IASI retrievals are most sensitive to CO ($\sim$ 450 hPa), stronger winds and a longer lifetime of CO than at the surface make the transport of CO over long distances possible.

Even if the signature of fire emissions on tropospheric CO fields is well seen, the existence of other sources than fires and the transport of fire emissions by atmospheric circulation make the study of the relation between fires and CO concentrations difficult. In order to highlight the links between fire activity and tropospheric CO, we now take advantage of the availability provided by infrared sounders to retrieve CO by both day and night.

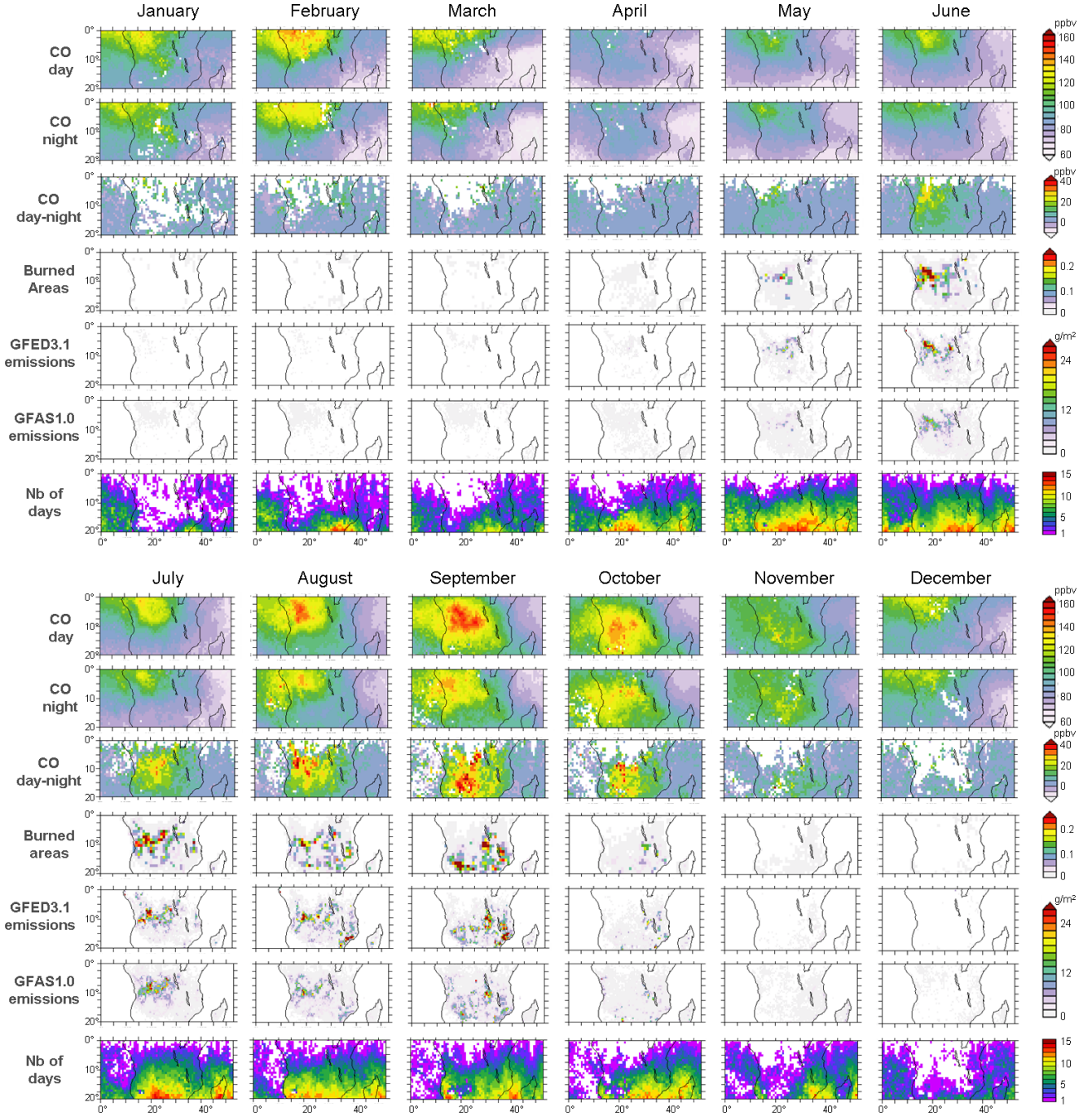

Figure 2. IASI CO and fires between January and December 2008 in southern Africa. From top to bottom: monthly means of the integrated content of CO from IASI, by day (09:30 LT) (in ppbv); by night (21:30 LT) (in ppbv); monthly means of the day–night differences of the integrated content of CO from IASI (in ppbv); MODIS burned areas (Roy et al., 2008) (in percent); GFED3.1 CO emissions (in $g\,m^{-2}$); GFAS1.0 CO emissions (in $g\,m^{-2}$); number of days for which the CO day–night difference is available.

3.2 A case study: diurnal variation of CO over southern Africa

3.2.1 IASI day- and night-time CO

We now focus on southern Africa (0–20° S, 0–53° E) which is an important region from a biomass burning perspective. Moreover, in contrast to northern Africa, southern Africa is rather preserved from strong pollution and dust events (Engelstaedter et al., 2006).

The first two rows of Fig. 2 show the monthly means of the integrated content of CO from IASI between January and December 2008, by day (09:30) and night (21:30), on a $0.75° \times 0.75°$ grid. The same spatiotemporal distribution of CO is seen on both time series. However, values of IASI CO by day are stronger than the ones by night. During the dry season, there is an excess of CO shifting progressively from the north-west in May to the south and south-east until November. This excess of tropospheric CO reaches a maximum in September–October. This evolution can be explained by the fire activity (Cahoon et al., 1992; Barbosa et al., 1999); it is similar to the evolution of the burned areas (BA) observed by Moderate Resolution Imaging Spectroradiometer (MODIS) (Collection 5; Roy et al., 2008) (Fig. 2, fourth row), as well as the evolution of fire emissions from GFED3.1 (Fig. 2, fifth row) and from GFAS1.0 (Fig. 2, sixth row), but with a shift of 1 to 2 months depending on the fire product considered. In addition, the excesses of CO in the troposphere are not located above the burned areas, suggesting that CO emitted by fires has been transported by convection and general atmospheric circulation.

The 2-month lag between the day/night retrieved CO and fires is observed for each of the 5 years studied here, as shown in Fig. 3, which represents the evolution of the monthly means of IASI CO by day and night, MODIS BA and CO emissions from GFED3.1 and GFAS1.0, in the same region as Fig. 2. It is worth noting that there are also disagreements between MODIS BA, GFED3.1 and GFAS1.0 emissions concerning the evolution of fires during the dry season. For example, according to GFED3.1, the maximum of the emissions generally occurs 1 month after the maximum of the burned areas. GFAS1.0 is lower than GFED3.1 and has a different interannual variability. These discrepancies are due to the fact that the emissions are not proportional to the burned areas and that many other variables have to be considered, like the type of vegetation, the combustion efficiency or the emission factor.

In April, which is a month of transition between the dry season in the north and the dry season in the south, IASI CO is minimum; it starts to increase in May, at the beginning of the fire season. In September–October, the maximum of the CO mixing ratio in the troposphere corresponds to the maximum of the GFED fire emissions in 2008 and 2011 but is 1 to 2 months delayed in the other years. In November, although fires are hardly active according to the MODIS BA, GFED3.1 and GFAS1.0, values of CO remain high.

Between December and March, i.e. outside of the fire season in the SH, high CO values are found between 0 and 5° S for both day and night. This is due to the southward transport of CO emitted by northern African fires. Such atmospheric processes complicate the analysis of the CO fields retrieved from space observations and our ability to disentangle the CO directly emitted by fire over the region of interest from the background and transported CO from nearby regions. This is why, following Chédin et al. (2005), we now focus on the analysis of the day–night difference of CO.

3.2.2 Day–night difference of IASI CO

Monthly means of day–night differences of CO are plotted in Fig. 2 (third row). It is computed as follows: first the $0.75° \times 0.75°$ daily means of the clear-sky retrievals of CO made at 09:30 and 21:30 are calculated; then, for each grid cell, the difference between 09:30 and 21:30 is computed for every day when both daytime and night-time retrievals are available, and then averaged over the whole month. Blank areas on the maps are due to a lack of points. The number of points available to compute the monthly means of day–night CO is plotted in Fig. 2 (seventh row). It shows that IASI orbits by day and night hardly, if not never, cross each other near the equator. During the wet season (i.e. from November to March), the number of points available to compute the monthly mean of day–night CO is also limited by the number of clear-sky observations available.

The 5-year evolution of the monthly means of the day–night differences of CO in southern Africa, along with the evolution of MODIS BA, GFED3.1 and GFAS1.0 emissions, is plotted in Fig. 4. Compared to the evolution of daytime and night-time CO (Fig. 3), the temporal evolution of the diurnal difference reaches a better agreement with fire activity. The maps of the diurnal difference show a positive signal between May and October which can exceed 40 ppbv. The day–night signal mostly captures CO above fires and follows their evolution between May and September, shifting towards south and south-east, with a maximum in September, at the same time as the emissions, or 1 month later. Between November and April, i.e. outside of the fire season, although the values of CO retrieved either by day or by night are quite high because of the transport from the NH, the day–night difference of CO is almost null. Over sea, the day–night difference is null. This suggests that the chosen differential approach emphasizes the CO emitted by fires while cancelling out the background CO stemming from CO emitted in other regions and then transported over the region of interest.

The retrieved diurnal signal is not always completely located just above fires as given by the different fire products. The same was observed for the DTE of CO_2: Rio et al. (2010) showed that the DTE was not always necessarily located just above the source, with the real DTE signal being sometimes

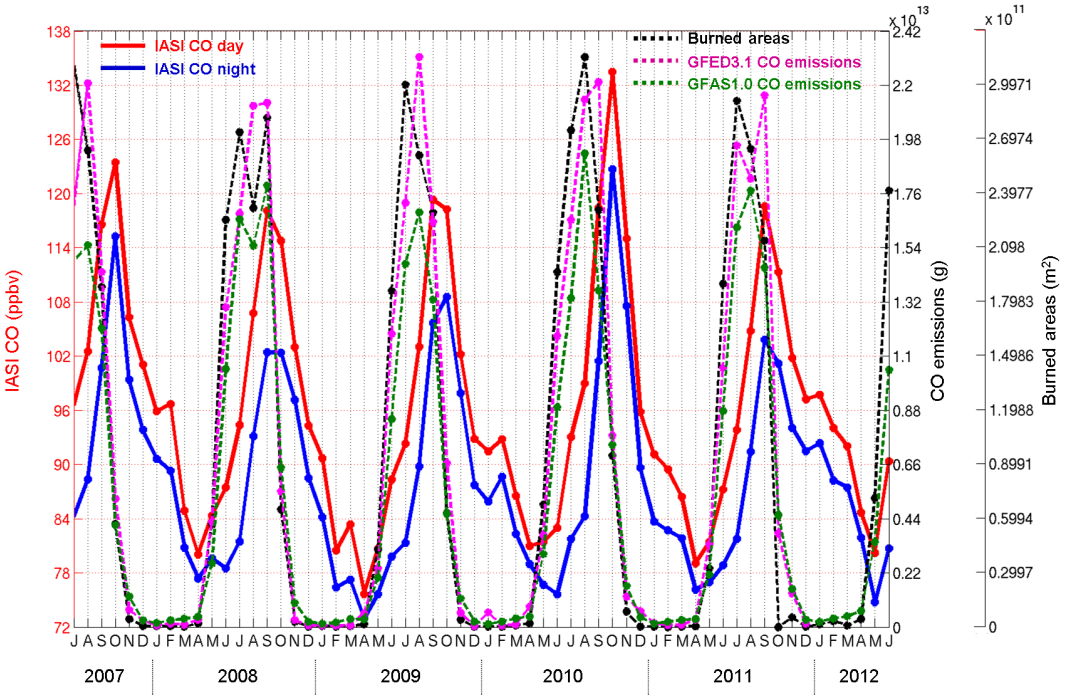

Figure 3. Evolution of the integrated content of CO from IASI on land and of fires between July 2007 and June 2012 in southern Africa (0–20° S, 0–53° E). Red: CO by day (09:30 LT). Blue: CO by night (21:30 LT). Black dashed: MODIS burned areas. Purple dashed: CO emissions from GFED3.1. Green dashed: CO emissions from GFAS1.0.

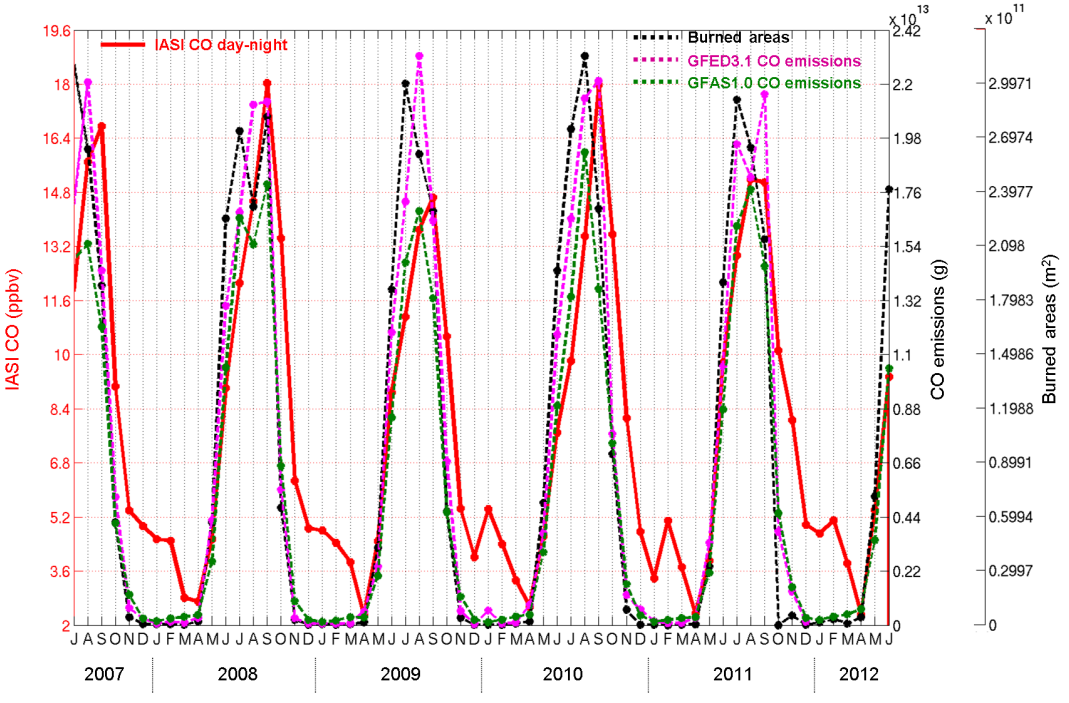

Figure 4. Evolution of the day–night difference of the integrated content of CO from IASI on land, and of fires, between July 2007 and June 2012 in southern Africa. Red: day–night CO. Black dashed: MODIS burned areas. Purple dashed: CO emissions from GFED3.1. Green dashed: CO emissions from GFAS1.0.

significant in surrounding areas, due to preferential directions of the large-scale advections. The DTE of CO_2 can even be negative on a daily scale due to particular horizontal winds. However, on a monthly basis, outside the source region, the DTE daily variations tend to cancel each other out. A distinction should thus be made between the influence of large-scale (and long-distance) transport that affects day and night IASI CO for months and the particular horizontal winds that can punctually affect the day minus night difference of CO. On monthly averages, the diurnal signal of CO is mostly located in the vicinity of the sources and will be interpreted here in relation to the region above which it is located.

Despite the good agreement between IASI diurnal CO and fire activity given by GFED3.1, GFAS1.0 emissions and MODIS burned areas (Fig. 2), there are some discrepancies between the two of them. For instance, between July and September, the day–night difference of IASI CO between 35 and 40° E is low despite the high level of burned areas seen by MODIS. Conversely, in October the diurnal difference is large even though fires are low. The decrease of the diurnal signal happens later than the decrease of fire activity; the signal is still substantial in November in 2010 and 2011 albeit fires are not active any more according to the fire products (Fig. 4). This kind of discrepancy in seasonality with an emission inventory has already been observed for this area with GFED2 (Edwards et al., 2006; van der Werf et al., 2006; Roberts et al., 2009). This lag could be due to the burning of woody fuels towards the end of the dry season, which may not be well represented in the inventory. These dense fuels emit large amounts of CO and are likely to burn on a long period. After the peak of the fire season, the smoldering phase of the combustion, which is characterized by thermodynamical conditions of higher moisture and lower temperature, favours CO emissions (Lobert and Warnatz, 1993) in fires that may not be captured in terms of burned area or FRP from space observations because of their small energy.

3.2.3 Relation between the day–night difference of CO and fire emissions

To study the diurnal cycle of CO in southern Africa and its relation with fires in more details, we focus on several areas represented in Fig. 5, whose coordinates are given in Table 1. These areas, adapted from Hoelzemann (2006), correspond to different emission source distributions, which can be linked to the different types of vegetation, which are also represented in Fig. 5, taken from Mayaux et al. (2003). The dominant types in southern Africa are forests, savannas and croplands. In these areas, we calculate the mean of the day–night difference of the integrated content of CO from IASI, whose evolution is represented in Fig. 6, on average between 2008 and 2011. Also plotted are the MODIS BA, the GFED3.1 and GFAS1.0 emissions for the same period.

There is a general agreement between the monthly evolution of the day–night difference of CO and the one of fire

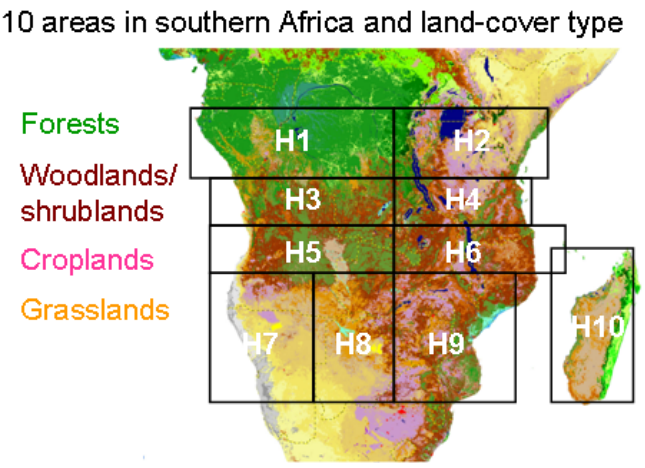

Figure 5. Definition of the studied areas in Africa, adapted from Hoelzemann (2006). Vegetation map is from Mayaux et al. (2003).

Table 1. Coordinates of the studied areas in southern Africa, corresponding to Fig. 5.

Code	Latitude	Longitude
H1	0–6° S	8–28° E
H2	0–6° S	28–43° E
H3	6–10° S	10–28° E
H4	6–10° S	28–40° E
H5	10–14° S	10–28° E
H6	10–14° S	28–43° E
H7	14–25° S	10–20° E
H8	14–25° S	20–28° E
H9	14–25° S	28–40° E
H10	12–25° S	42–50° E

emissions for most of the selected areas. It is visible for areas H4 and H6, concerning both the seasonality and the intensity of the signals. For areas H7 and H8, dominated by grasslands, there is a good agreement in the seasonality, but the amplitude of the day–night CO is strong whereas GFED and GFAS fire emissions and MODIS BA are low. On the contrary, for H9, an area dominated by croplands, the day–night CO is lower than the GFED3.1 signal, but fits GFAS1.0. H10, Madagascar, is characterized by almost no fire activity; as a result the day–night CO is low and constant, in agreement with the MODIS BA, GFED3.1 and GFAS1.0 emissions.

According to MODIS BA, GFED3.1 and GFAS1.0 emissions, areas H3 and H5 are those where most fire activity is observed. They are also the ones for which the day–night difference of CO is strongest. As for the fire season, the increase in the diurnal signal of CO begins in May. However the maximum is reached 1 month later than the maximum of the emissions, and high values remain until October although fires are not active any more according to the three fire products. The lag between the diurnal variation of CO

and the two fire products observed over the whole southern Africa (cf. Sect. 3.2.2), thus only takes place in these two areas mostly occupied by forests and wooden savannas.

Areas H1 and H2, in the north of the region, display the worst agreement: the background level of the diurnal signal is high and there is a shift of 1 month of the seasonality compared to fires. However, as seen in Fig. 2, these areas are only covered by a few points, and the monthly means in these areas are calculated from the few days where the day–night difference of CO is available.

To conclude, the agreement in seasonality and intensity between fire activity and the diurnal cycle of CO in southern Africa shown in Fig. 4 is the result of an agreement between these signals at finer scales, where different kinds of vegetation prevail. The comparison is limited near the equator by the number of observations available to compute a significant day–night difference of CO.

3.3 Link between day–night CO and fire emissions in the tropics

We now extend our study to the tropical zone, which is divided into 12 areas plotted in Fig. 7 and defined in Table 2. These areas are taken from Chédin et al. (2008) and are representative of the different fire seasons. Figure 8 compares the annual means of the day–night difference of CO (in ppbv) with the annual means of the GFED3.1 and GFAS1.0 emissions (in $\mathrm{gCO\,m^{-2}}$), averaged over 2008–2011. It can be compared to Fig. 11 from Chédin et al. (2008) that shows the annual GFED2 CO_2 emissions as a function of the DTE of CO_2 computed from the TOVS observations.

Both with GFED and GFAS, a linear relationship can be seen between the two variables over a large interval, between 3 and 15 ppbv. This relationship supports the interpretation of the day–night difference of CO as a signal directly related to biomass burning emissions. GFAS1.0 displays a better agreement with the diurnal signal of CO than GFED3.1, mainly because of lower emissions in the south-eastern Africa (AfSE) area (see also the area H9 in Fig. 6). Otherwise, two areas stand out: north-east and central Africa (AfNEC), with a low diurnal signal, and Central America (AmC), with a high diurnal signal, compared to the emissions. Despite these two areas, the correlation is high between the diurnal signal of CO on the one hand and the GFED3.1 emissions ($R^2 \sim 0.6$) and the GFAS1.0 emissions ($R^2 \sim 0.7$) on the other hand. However it is lower than the correlation between the DTE of CO_2 and the emissions found by Chédin et al. (2008) ($R^2 \sim 0.8$).

As stressed by Chédin et al. (2008) for CO_2, the discrepancies between the emissions and the diurnal signal in the troposphere can be related to the atmospheric transport or complex diurnal cycles of the emissions. They also may come from a mischaracterization of the specificity of CO emissions in fire inventories, especially from the smoldering fire phase. In particular, most of emission factors are based on averages per biome that do not take into account temporal and spatial variability, although they are influenced by several environmental factors.

4 Discussion

4.1 Impact of the vertical sensitivity of the sounder on the day–night difference of CO

As seen in Fig. 4 (or Fig. 6), the diurnal excess of CO is still positive outside of the fire season, even if it stays low. Given that there is no other significant diurnal source of CO in southern Africa, these signals can be explained by the diurnal variation of the vertical sensitivity of the CO retrieval. As seen in Fig. 9, which represents the IASI CO weighting functions in southern Africa, the weighting functions during daytime display a higher sensitivity to CO close to the surface, due to a higher thermal contrast (i.e. the difference between the surface temperature and the temperature of the first pressure level), during and outside of the fire season (July and January, respectively) (Thonat et al., 2012).

However, the comparison between both monthly maps of thermal contrast conditions and CO day–night differences over southern Africa in July 2008 (Fig. S1 in the Supplement) reveals that diurnal signals of CO and thermal contrast have quite different spatial distributions. On the continent, the day–night difference of the thermal contrast is everywhere positive and exceeds 20 K west and south-west of the area, where the day–night CO is not at its highest. And the day–night CO reaches its maximum values for an average day–night difference of the thermal contrast.

This result is confirmed by Fig. 10, which represents scatter plots of IASI CO retrievals vs. the thermal contrast, spot by spot, for daytime observations (Fig. 10a) and night-time observations (Fig. 10b), as well as day–night IASI CO vs. the daytime thermal contrast (Fig. 10c) and vs. the diurnal variations of the thermal contrast (Fig. 10d), between June and October 2008 in southern Africa. A high/low thermal contrast does not necessarily lead to a high/low IASI CO retrieval, by day or by night. The same is true for the day–night difference of CO, even thought the thermal contrast is generally higher in the daytime that in the night-time. Moreover, values of the diurnal signal of CO higher than 10 ppbv, which are the ones that are mostly related to fires, correspond to a wide range of daytime thermal contrast or of its diurnal variation, yielding a correlation close to 0 between CO diurnal variation and thermal contrast.

As was explained in Sect. 2.2, the retrieved tropospheric column of CO $q\mathrm{CO}$ is the sum of the integrated content of the input profile of the radiative transfer model 4A and of the excess (or deficit) of CO estimated in respect to it. This means

$$q\mathrm{CO} = q\mathrm{CO}^{4\mathrm{A}} + \Delta q\mathrm{CO} \quad (2)$$

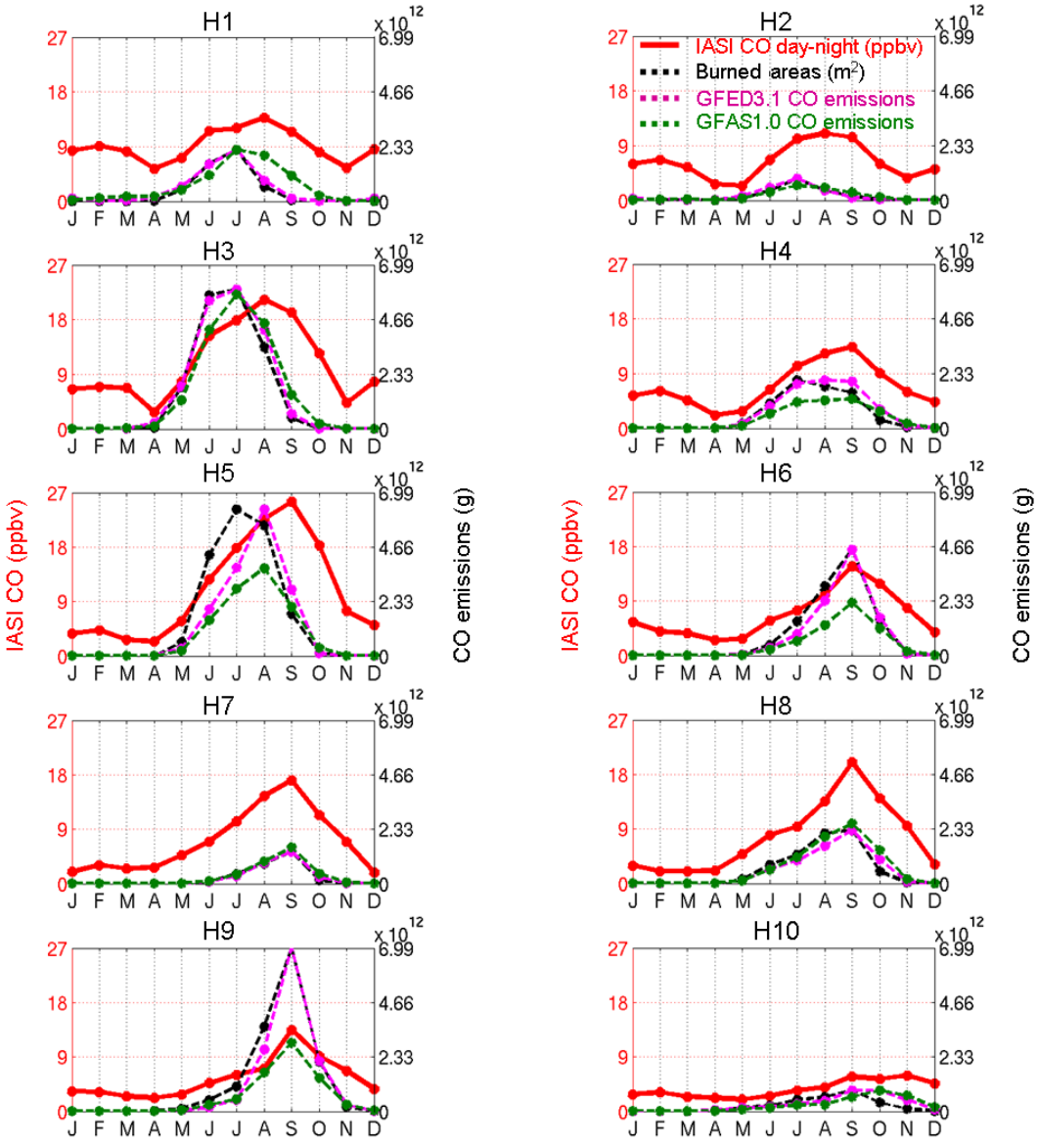

Figure 6. Evolution of the day–night difference of the integrated content of CO from IASI on land, and of fires, on average over 2008–2011 on different areas in southern Africa (see Fig. 5). Red: day–night CO. Black dashed: MODIS Burned Areas. Purple dashed: CO emissions from GFED3.1. Green dashed: CO emissions from GFAS1.0.

Table 2. Coordinates of the studied areas in the tropics, corresponding to Fig. 7. Af, Am and Aus respectively stand for Africa, America and Australia. N, S, E and W respectively stand for north, south, east and west, and t stands for total.

Code	Latitude	Longitude	Code	Latitude	Longitude
AfNW	15–0° N	20° W to 20° E	AfSE	0–20° S	25–40° E
AfNE	15–0° N	30–45° E	AfSt	0–25° S	10–40° E
AfNEC	15–0° N	20–45° E	Aft	25° N to 25° S	20° W to 43° E
AfN	15–0° N	20° W to 45° E	AmSE	0–25° S	60–35° W
AfNt	25–0° N	20° W to 45° E	AmC	25–0° N	110–62° W
AfSW	0–20° S	10–25° E	Aus	12-25° S	110–160° E

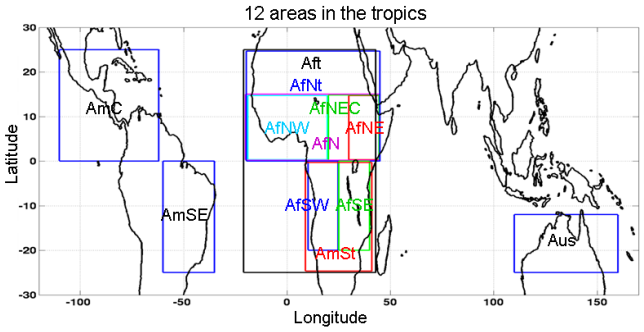

Figure 7. Definition of the studied areas in the tropics. Adapted from Chédin et al. (2008). Only lands are considered. Af, Am and Aus respectively stand for Africa, America and Australia. N, S, E and W respectively stand for north, south, east and west, and t stands for total.

The first term of this sum is given by

$$q\mathrm{CO}^{4\mathrm{A}} = \sum_{i=1}^{42} \mathrm{wf}_i \times \mathrm{profileCO}_i^{4\mathrm{A}}, \quad (3)$$

where i is the number of the pressure layer, wf is the weighting function of CO for the given retrieval (in ppbv ppbv^{-1}) and profile CO$^{4\mathrm{A}}$ is the profile used as input in 4A for every simulation. profileCO$^{4\mathrm{A}}$ corresponds to average CO conditions: it is constant, equal to 97 ppbv, from the surface to 584 hPa.

Figure 11 shows the evolution of the day–night difference of qCO$^{4\mathrm{A}}$, on the same period and in the same area as in Fig. 4. Given that only one profile is used as input in 4A, the diurnal signal in Fig. 11 is only due to the diurnal variations of the weighting function. Naturally, the second term of the sum in Eq. (2), ΔqCO, is also dependent on the weighting function. However, quantifying the impact of the diurnal variations of the weighting function on this term (thus on qCO) would require to know the "true" profiles of CO corresponding to the passes of the sounder, whether these profiles come from observations or simulations of a chemistry-transport model. That is why here we only focus on the day–night difference of qCO$^{4\mathrm{A}}$, which gives an approximation of the influence of the weighting functions and can be compared to the diurnal signal of CO in Fig. 4.

As expected, the signal is positive and has almost the same seasonality as the diurnal signal shown in Fig. 4, with a shift of 1 month. It is about 5 ppbv between December and April, which coarsely corresponds to the bias observed in Fig. 4 for these months, April excepted. In addition, the amplitude of the signal in Fig. 11 is only about 2 ppbv whereas the amplitude of the day–night difference of CO is 15 ppbv (Fig. 4).

In order to evaluate the impact of the choice of the reference profile profileCO$^{4\mathrm{A}}$ on the vertical sensitivity and the diurnal signal of CO, we have performed the same analysis as above assuming a profile characterized by enhanced concentration of CO near the surface: 500 ppbv at the surface and 300 ppbv at the first level above the surface (Fig. S2).

The resulting day–night difference of qCO$^{4\mathrm{A}}$ obtained using this strongly polluted profile of CO in the retrieval procedure is plotted in Fig. 11 as blue points for each January, April, July and October between 2008 and 2012. As expected, with the polluted profile, the day–night difference of qCO$^{4\mathrm{A}}$ is higher than with the reference profile (red curve). However, it is still low compared to the diurnal signal of CO plotted in Fig. 4 (red curve). Moreover, the amplitude of the signal has only increased by less than 1 ppbv despite the very high values of CO assumed near the surface. Similar conclusions have been obtained with even more strongly polluted profile (not shown).

Although this experiment is an approximation of the influence of the variations of the vertical sensitivity between night and day, these results strongly suggest that the diurnal tropospheric excess of CO retrieved from IASI is mostly due to the diurnal cycle of fire emissions.

4.2 Hypothesis on the mechanisms explaining the relation between fires and the day–night difference of CO

As exposed in Sect. 3.3, the diurnal signals of CO and CO_2 are of opposite signs: Chédin et al. (2008) have shown that CO_2 concentrations in the troposphere are higher by night, whereas we find here that CO concentrations are higher in the daytime. Several factors can explain this sign difference.

As stated above, CO and CO_2 are emitted during the flaming and the smoldering phases of the combustion, in which their emissions are anti-correlated. The flaming phase favours CO_2 emissions (Lobert and Warnatz, 1993); it is characterized by high temperatures (800–1200 °C) (Pyne et al., 1996) which entail strong uprisings and is associated with the combustion of the aboveground biomass. So, during the day in this phase, fires emit large quantities of CO_2 reaching the high troposphere. At the end of the day, the infrared sounder's measurements, which are representative of the high troposphere, allow to observe this accumulation of fire emissions under the tropopause. Conversely, at the beginning of the day, after the emissions have been diluted and before fires start again (or before the emissions can reach such altitudes), the sounder only observes the background level of CO_2 (Chédin et al., 2005, 2008).

The other phase of the combustion, the smoldering phase, favours CO emissions (Lobert and Warnatz, 1993); it is characterized by lower temperatures (100–600 °C) (Pyne et al., 1996), which contribute to more stable plumes, more prone to be driven by the variability of the boundary layer; it is associated with the combustion of the organic layer. At the end of the day, still active fires lose their efficiency, favouring CO emissions in the smoldering phase (Ward et al., 1996; Kasischke and Bruhwiler, 2003).

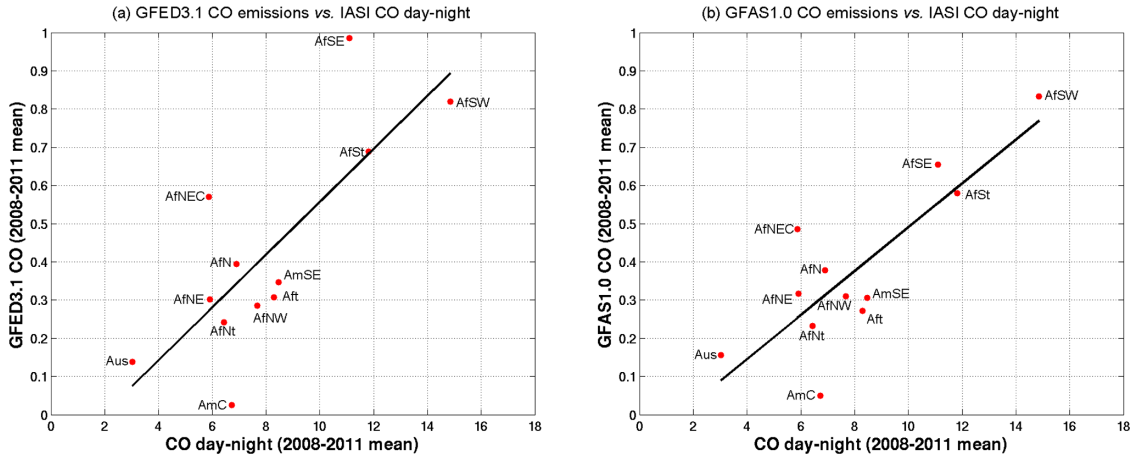

Figure 8. (a) GFED3.1 and **(b)** GFAS1.0 emissions (in $gCO\,m^{-2}$) as a function of the day–night difference of the integrated content of CO from IASI (in ppbv) in different tropical areas (see Fig. 7), on average over 2008–2011.

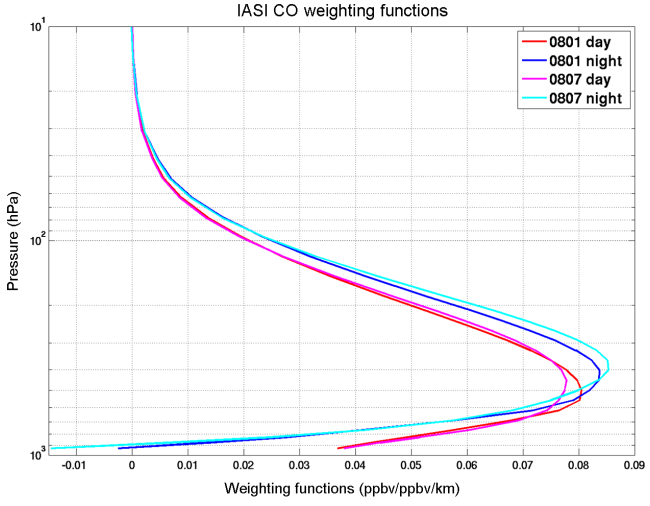

Figure 9. IASI CO weighting functions ($ppbv\,ppbv^{-1}\,km^{-1}$), averaged over southern Africa, on land. Red: January by day (09:30 LT). Blue: January by night (21:30 LT). Magenta: July by day. Cyan: July by night.

The fact that the smoldering phase can last long, with CO plumes staying close to the surface, entails high CO concentrations in the first layers, in particular at night. For example, Ferguson et al. (2003) measured in Alaska extreme CO concentrations at midnight, reaching 27 ppmv, between 0 and 150 m altitude. These extreme concentrations are the consequence of a very stable boundary layer. Ferguson et al. (2003) observed almost no smoke at about 2000 m. The day after, fires were less active, and the concentrations were much lower, of the order of a ppmv. The extreme concentrations of the previous day were dissipated by the natural convection and advection. Even though this is an example of a boreal forest fire, it highlights the possibility that, while fires can be very active during the day, with emissions reaching the free troposphere, the majority of the smoke is trapped at low altitudes at night and then uplifted in the morning by the natural convection and the pyroconvection.

Figure 12 shows the mean boundary layer height in southern Africa and South America, between July and November 2008, i.e. during the fire season, calculated from the ECMWF forecasts. The boundary layer behaves the same way during these months, but the maximum of the height, reached in the early afternoon, increases from July to September and then decreases until November. The boundary layer is always low, at about 200 m, between 19:30 and 04:30. The natural convection becomes important only after 07:30. When IASI passes at 21:30, night-time CO emissions are trapped in the boundary layer so they are not visible by the sounder, which is sensitive to CO in the mid-troposphere and insensitive to CO close to the surface by night, as shown in Fig. 9. When IASI passes at 09:30, the trapped CO has been uplifted by natural convection and reaches altitudes to which the sounder is sensitive to CO. In addition, at 09:30, fires are active again (mostly in the flaming phase of the combustion), with strong vertical movements that can uplift surrounding smokes. As a result, above burning areas, the day–night difference of CO computed from IASI is a positive signal directly related to fire emissions.

These different factors support the hypothesis of the convection of CO emissions in the mid-troposphere in the morning, following their accumulation in the boundary layer during the night. The sign difference between the diurnal signals of CO and CO_2 is the result of the specificity of the two phases of the combustion and of the difference in the sounder's vertical sensitivity to these two gases.

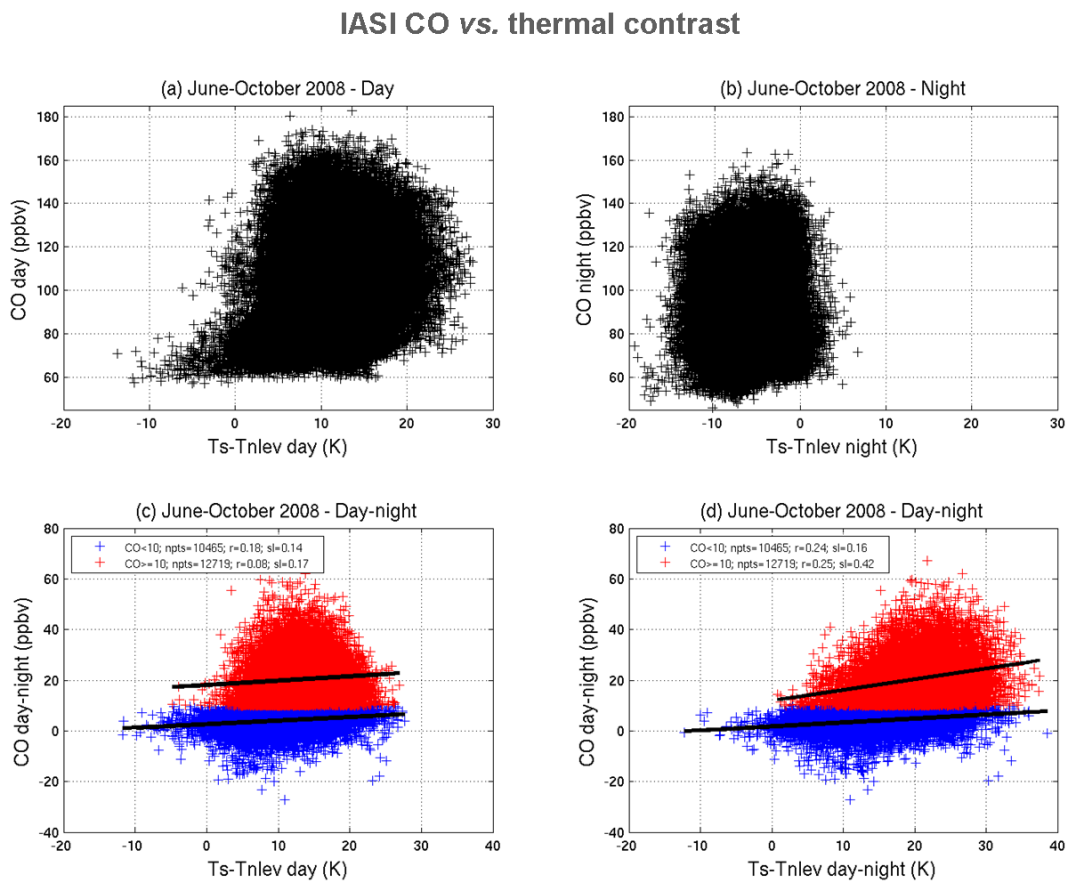

Figure 10. (a) IASI CO (in ppbv) by day as a function of the thermal contrast (in K), between June and October 2008, in southern Africa, on land. **(b)** Same as **(a)**, by night. **(c)** Day–night difference of IASI CO (in ppbv) as a function of the thermal contrast by day (in K). **(d)** Same as **(c)** for the day–night difference of the thermal contrast.

5 Conclusion

The relation between tropical biomass burning emissions and CO has been analysed by interpreting 5 years (2007–2012) of tropospheric CO column retrieved from IASI observations by day and by night (09:30/21:30 LT) and temporal series of burned areas (MODIS) and fire emissions (GFED3.1 and GFAS1.0). Following Chédin et al. (2005, 2008) who related the diurnal signature of CO_2 retrieved from NOAA10/TOVS instruments to fire emissions, we have taken advantage of the fact that IASI overpasses every point twice a day, before and after the maximum of the diurnal cycle of fires, in order to relate directly fires and CO concentrations in the troposphere.

The spatiotemporal evolution of the diurnal signal of tropospheric CO as retrieved from IASI, defined here as the day–night difference of CO, displays a better agreement with the evolution of fires compared to CO by day or by night only. This differential approach cancels out the background CO, including plumes due to advective transport from nearby regions, and is only sensitive to the CO related to local fire emissions. A linear relationship is found over various regions in the tropics between the diurnal difference of IASI CO and CO fire emissions from the GFED3.1 ($R^2 \sim 0.6$) and GFAS1.0 ($R^2 \sim 0.7$) inventories. For regions near the equator, daytime and night-time orbits of the sounder overlap less, inducing a limited number of clear-sky spots available.

Some discrepancies arise between emissions from GFED3.1 and GFAS1.0 and IASI CO in southern Africa. In terms of seasonality, in regions of wooden savannas, the fire activity suggested by the IASI day–night difference of CO is more intense towards the end of the fire season (September) than GFED3.1 and GFAS1.0 emissions indicate. It might be due to the fact that these regions with dense fuel are likely to favour carbon emissions during the smoldering phase up until the end of the fire season. In terms of intensity, this could indicate that the specificity of CO emissions compared to CO_2 emissions for each biome might need to be refined in the emission inventory's framework.

The diurnal signals of CO_2 from TOVS (Chédin et al., 2005, 2008) and CO from IASI are of opposite signs. CO retrievals are indeed higher in the daytime than in the nighttime. The suggested mechanism explaining the diurnal signal of CO is as follows: CO is emitted in large quantities in

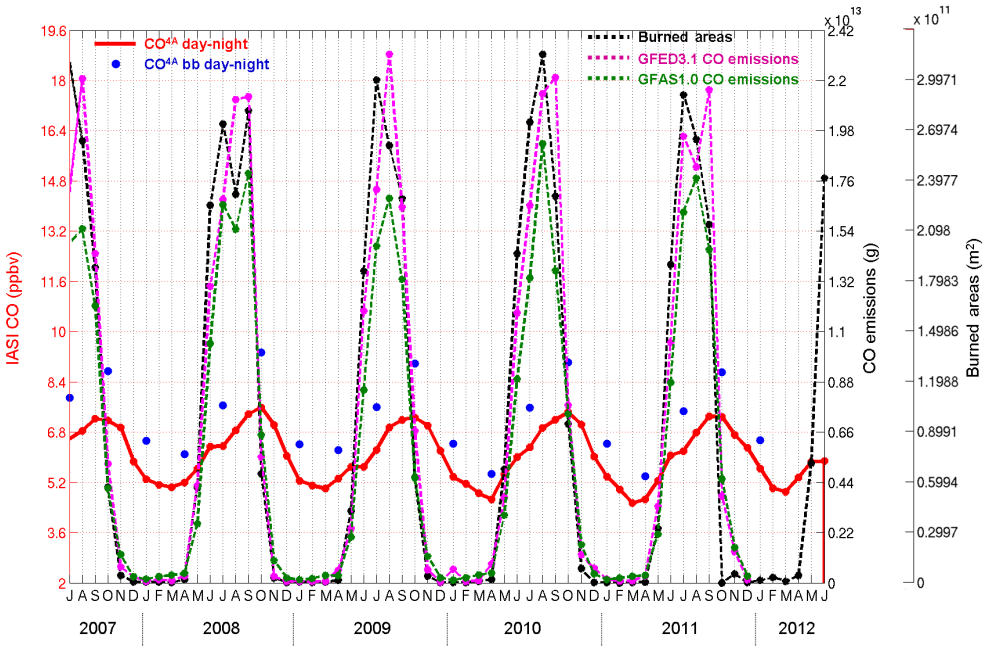

Figure 11. Evolution of the day–night difference of the integrated content $q\mathrm{CO}^{4A}$ (see text Sect. 4.1) on land, and of fires, between July 2007 and June 2012 in southern Africa. Red: day–night difference of $q\mathrm{CO}^{4A}$. Blue dots: day–night difference of $q\mathrm{CO}^{4A}$ computed with a polluted CO profile as input in 4A. Black dashed: MODIS burned areas. Purple dashed: CO emissions from GFED3.1. Green dashed: CO emissions from GFAS1.0.

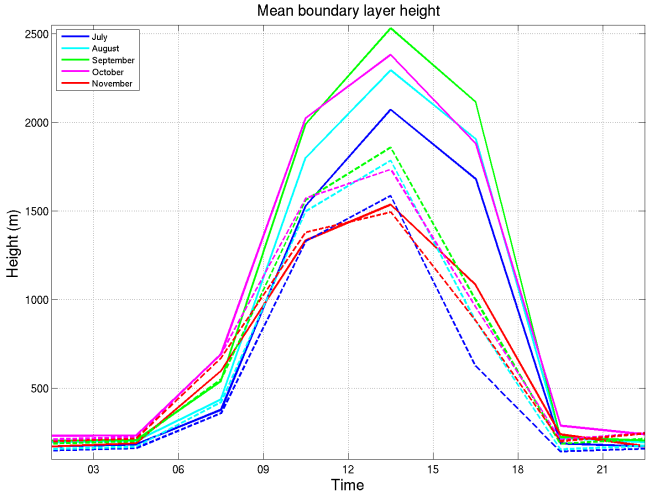

Figure 12. Mean boundary layer height in southern Africa (solid line) and South America (dashed lines) between July and November 2008. Plotted from the ECMWF forecasts, which have a 3 h time step and a $0.75° \times 0.75°$ spatial resolution.

the smoldering phase of the combustion occurring during the night (after that fires in the flaming phase have burned the above ground vegetation in the daytime) and accumulates in the boundary layer, until being uplifted from the beginning of the day. This hypothesis is supported both by the specificity of CO emissions compared to CO_2 emissions as well as by the fact that the retrievals of these gases are not representative of the same part of the atmosphere. Simulations with general circulation models should help to validate the plausibility of this mechanism and to compare the effects of vertical transport patterns related to the different combustion phases on the injection of CO and CO_2 in the mid- and upper troposphere. The results presented here show that the analysis of diurnal variations of CO and CO_2 as measured from space can give us a global view of the repartition of the emissions between the flaming and the smoldering phase and of their associated transport, which need to be taken into account in surface flux estimation procedures and emission inventories.

The monitoring of CO from space with our retrieval method can be extended to IASI observations on Metop-B, which was launched in 2012, and Metop-C, which will be launched in 2017, providing at least 20 years of observations at the same passing times. As part of the EUMETSAT Polar System-Second Generation (EPS-SG) program, IASI-New Generation (IASI-NG, Crevoisier et al., 2014) will cover the period 2020–2042 on the same orbit as IASI, allowing us to study long term the evolution of CO, its diurnal cycle and its relation with fires. Our CO retrieval method can also be applied to Aqua/AIRS observations (see Thonat et al., 2012), whose passing times are 01:30/13:30, giving us four points in the diurnal cycle of CO. CrIs, with the same characteristics as AIRS, was launched in 2011 and will also be on the Joint Polar Satellite System (JPSS) program planned for 2017. Since IASI enables the retrieval of other gases emitted

by fires such as CO_2 and CH_4, it also gives the opportunity of a multispecies study that can provide a more accurate view of the specificities of fire emissions.

The Supplement related to this article is available online at doi:10.5194/acp-15-13041-2015-supplement.

Acknowledgements. This research was supported by Centre National d'Etudes Spatiales (CNES, France) and Microsoft Research Ltd. This work has also been supported by the Agence Nationale de la Recherche under contract 2010 BLAN 611 01 "TropFire". IASI has been developed and built under the responsibility of CNES. It is flown on-board the Metop satellites as part of the EUMETSAT Polar System. The IASI L1 data are received through the EUMETCast near-real-time data distribution service. We particularly wish to thank the ETHER centre team for their help in getting IASI data. Calculations were performed using the resources of IDRIS, the computing centre of CNRS, of ECMWF and of the IPSL data and computing centre ClimServ.

Edited by: I. Aben

References

Andreae, M. O.: Biomass burning: Its history, use and distribution and its impacts on environmental quality and global climate, in: Global Biomass Burning: Atmospheric, Climatic, and Biospheric Implications, edited by: Levine, J. S., MIT Press, Cambridge, 3–21, 1991.

Andreae, M. O., Rosenfeld, D., Artaxo, P., Costa, A. A., Frank, G. P., Longo, K. M., and Silva-Dias, M. A. F.: Smoking Rain Clouds over the Amazon, Science, 303, 1337–1342, doi:10.1126/science.1092779, 2004.

Barbosa, P. M., Stroppiana, D., Grégoire, J. M., and Pereira, J. M. C.: An assessment of vegetation fire in Africa (1981–1991): burned areas, burned biomass, and atmospheric emissions, Global Biogeochem. Cy., 13, 933–950, 1999.

Bowman, D. M. J. S., Balch, J. K., Artaxo, P., Bond, W. J., Carlson, J. M., Cochrane, M. A., D'Antonio, C. M., DeFries, R. S., Doyle, J. C., Harrison, S. P., Johnston, F. H., Keeley, J. E., Krawchuk, M. A., Kull, C. A., Marston, J. B., Moritz, M. A., Prentice, I. C., Roos, C. I., Scott, A. C., Swetnam, T. W., van der Werf, G. R., and Pyne, S. J.: Fire in Earth System, Science, 324, 481–484, 2009.

Brenninkmeijer, C. A. M., Crutzen, P., Boumard, F., Dauer, T., Dix, B., Ebinghaus, R., Filippi, D., Fischer, H., Franke, H., Frieß, U., Heintzenberg, J., Helleis, F., Hermann, M., Kock, H. H., Koeppel, C., Lelieveld, J., Leuenberger, M., Martinsson, B. G., Miemczyk, S., Moret, H. P., Nguyen, H. N., Nyfeler, P., Oram, D., O'Sullivan, D., Penkett, S., Platt, U., Pupek, M., Ramonet, M., Randa, B., Reichelt, M., Rhee, T. S., Rohwer, J., Rosenfeld, K., Scharffe, D., Schlager, H., Schumann, U., Slemr, F., Sprung, D., Stock, P., Thaler, R., Valentino, F., van Velthoven, P., Waibel, A., Wandel, A., Waschitschek, K., Wiedensohler, A., Xueref-Remy, I., Zahn, A., Zech, U., and Ziereis, H.: Civil Aircraft for the regular investigation of the atmosphere based on an instrumented container: The new CARIBIC system, Atmos. Chem. Phys., 7, 4953–4976, doi:10.5194/acp-7-4953-2007, 2007.

Buchwitz, M., Khlystova, I., Bovensmann, H., and Burrows, J. P.: Three years of global carbon monoxide from SCIAMACHY: comparison with MOPITT and first results related to the detection of enhanced CO over cities, Atmos. Chem. Phys., 7, 2399–2411, doi:10.5194/acp-7-2399-2007, 2007.

Cahoon, D. R., Stocks, B. J., Levine, J. S., Coter III, W. R., and O'Neill, C. P.: Seasonal distribution of African fires, Nature, 359, 812–815, 1992.

Chédin, A., Serrar, S., Scott, N. A., Pierangelo, C., and Ciais, P.: Impact of tropical biomass burning emission on the diurnal cycle of upper tropospheric CO_2 retrieved from NOAA 10 satellite observations, J. Geophys. Res., 110, D11309, doi:10.1029/2004JD005540, 2005.

Chédin, A., Scott, N. A., Armante, R., Pierangelo, C., Crevoisier, C., Fossé, O., and Ciais, P.: A quantitative link between CO_2 emissions from tropical vegetation fires and the daily tropospheric excess (DTE) of CO_2 seen by NOAA-10 (1987–1991), J. Geophys. Res., 113, D05302, doi:10.1029/2007JD008576, 2008.

Crevoisier, C., Chédin, A., Heilliette, S., Scott, N. A., Serrar, S., and Armante, R.: Mid-tropospheric CO_2 retrieval in the tropical zone from AIRS observations, Proceedings of the 13th International TOVS Study Conference, St. Adele, Canada, 29 October to 4 November, https://cimss.ssec.wisc.edu/itwg/itsc/itsc13/proceedings/ (last access: 23 November 2015), 2003.

Crevoisier, C., Clerbaux, C., Guidard, V., Phulpin, T., Armante, R., Barret, B., Camy-Peyret, C., Chaboureau, J.-P., Coheur, P.-F., Crépeau, L., Dufour, G., Labonnote, L., Lavanant, L., Hadji-Lazaro, J., Herbin, H., Jacquinet-Husson, N., Payan, S., Péquignot, E., Pierangelo, C., Sellitto, P., and Stubenrauch, C.: Towards IASI-New Generation (IASI-NG): impact of improved spectral resolution and radiometric noise on the retrieval of thermodynamic, chemistry and climate variables, Atmos. Meas. Tech., 7, 4367–4385, doi:10.5194/amt-7-4367-2014, 2014.

Duncan, B. N., Martin, R. V., Staudt, A. C., Yevich, R., and Logan, J. A.: Interannual and seasonal variability of biomass burning emissions constrained by satellite observations, J. Geophys. Res., 108, 4100, doi:10.1029/2002JD002378, 2003.

Duncan, B. N., Logan, J. A., Bey, I., Megretskaia, I. A., Yantosca, R. M., Novelli, P. C., Jones, N. B., and Rinsland, C. P.: Global budget of CO, 1988-1997: Source estimates and validation with a global model, J. Geophys. Res., 112, D22301, doi:10.1029/2007JD008459, 2007.

Edwards, D. P., Emmons, L. K., Gille, J. C., Chu, A., Attié, J.-L., Giglio, L., Wood, S. W., Haywood, J., Deeter, M. N., Massie, S. T., Ziskin, D. C., and Drummond, J. R.: Satellite-observed pollution from Southern Hemisphere biomass burning, J. Geophys. Res., 111, D14312, doi:10.1029/2005JD006655, 2006.

Engelstaedter, S., Tegen, I., and Washington, R.: North African dust emissions and transport, Earth-Sci. Rev., 79, 73–100, 2006.

Ferguson, S. A., Collins, R. L., Ruthford, J., and Fukuda, M.: Vertical distribution of nighttime smoke following a wildland biomass fire in boreal Alaska, J. Geophys. Res., 108, 4743, doi:10.1029/2002JD003324, 2003.

Freeborn, P. H., Wooster, M. J., Hao, W. M., Ryan, C. A., Nordgren, B. L., Baker, S. P., and Ichoku, C.: Relationships between en-

ergy release, fuel mass loss, and trace gas and aerosol emissions during laboratory biomass fires, J. Geophys. Res., 113, D01301, doi:10.1029/2007JD008679, 2008.

Freitas, S. R., Longo, K. M., and Andreae, M. O.: Impact if including the plume rise of vegetation fires in numerical simulations of associated atmospheric pollutants, Geophys. Res. Lett., 33, L17808, doi:10.1029/2006GL026608, 2006.

Giglio, L.: Characterization of the tropical diurnal fire cycle using VIRS and MODIS observations, Remote Sens. Environ., 108, 407–421, doi:110.16/j.rse.2006.11.018, 2007.

Guan, H., Chatfield, R. B., Freitas, S. R., Bergstrom, R. W., and Longo, K. M.: Modeling the effect of plume-rise on the transport of carbon monoxide over Africa with NCAR CAM, Atmos. Chem. Phys., 8, 6801–6812, doi:10.5194/acp-8-6801-2008, 2008.

Hilton, F., Armante, R., August, T., Barnet, C., Bouchard, A., Camy-Peyret, C., Capelle, V., Clarisse, L., Clerbaux, C., Coheur, P.-F., Collard, A., Crevoisier, C., Dufour, G., Edwards, D., Faijan, F., Fourrié, N., Gambacorta, A., Goldberg, M., Guidard, V., Hurtmans, D., Illingworth, S., Jacquinet-Husson, N., Kerzenmacher, T., Klaes, D., Lavanant, L., Masiello, G., Matricardi, M., McNally, A., Newman, S., Pavelin, E., Payan, S., Péquignot, E., Peyridieu, S., Phulpin, T., Remedios, J., Schlüssel, P., Serio, C., Strow, L., Stubenrauch, C., Taylor, J., Tobin, D., Wolf, W., and Zhou, D.: Hyperspectral Earth Observation from IASI: four years of accomplishments, B. Am. Meteorol. Soc., 93, 347–370, doi:10.1175/BAMS-D-11-00027.1, 2012.

Hoelzemann, J. J., Schultz, M. G., Brasseur, G. P., Granier, C., and Simon, M.: Global Wildland fire Emission Model (GWEM): Evaluating the use of global area burnt satellite data, J. Geophys. Res., 109, D14S04, doi:10.1029/2003JD003666, 2004.

Hoelzemann, J. J.: Global Wildland Fire Emission Modeling for Atmospheric Chemistry Studies, PhD thesis, Max Planck Institute for Meteorology/University of Hamburg, Germany, Reports 5 on Earth System Science, 28/2006, ISSN 1614-1199, 2006.

Holloway, T., Levy II, H., and Kasibhatla, P.: Global distribution of carbon monoxide, J. Geophys. Res., 105, 12123–12147, 2000.

IPCC: Climate Change 2007: The Physical Science Basis. Contribution of Working Group I to the Fourth Assessment Report of the Intergovernmental Panel on Climate Change, edited by: Solomon, S., Qin, D., Manning, M., Chen, Z., Marquis, M., Averyt, K. B.,Tignor, M., and Miller, H. L., Cambridge University Press, Cambridge, United Kingdom and New York, NY, USA, 2007.

Ito, A. and Penner, J. E.: Global estimates of biomass burning emissions based on satellite imagery for the year 2000, J. Geophys. Res., 109, D14S05, doi:10.1029/2003JD004423, 2004.

Jain, A. K., Tao, Z., Yang, X., and Gillepsie, C.: Estimates of global biomass burning emissions for reactive greenhouse gases (CO, NMHCs, and NO_x) and CO_2, J. Geophys. Res., 111, D06304, doi:10.1029/2005JD006237, 2006.

Kaiser, J. W., Heil, A., Andreae, M. O., Benedetti, A., Chubarova, N., Jones, L., Morcrette, J.-J., Razinger, M., Schultz, M. G., Suttie, M., and van der Werf, G. R.: Biomass burning emissions estimated with a global fire assimilation system based on observed fire radiative power, Biogeosciences, 9, 527–554, doi:10.5194/bg-9-527-2012, 2012.

Kasischke, E. S. and Bruhwiler, L. P.: Emissions of carbon dioxide, carbon monoxide, and methane from boreal forest fires in 1998, J. Geophys. Res., 108, 8146, doi:10.1029/2001JD000461, 2003.

Langenfelds, R. L., Francey, R. J., Pak, B. C., Steele, L. P., Llyod, J., Trudinger, C. M., and Allison, C. E.: Interannual growth rate variations of atmospheric CO_2 and its $\delta^{13}C$, H_2, CH_4, and CO between 1992 and 1999 linked to biomass burning, Global Biogeochem. Cy., 16, 1048, doi:10.1029/2001GB001466, 2002.

Lavoué, D., Liousse, C., Cahier, H., Stocks, B. J., and Goldammer, J. G.: Modeling of carbonaceous particles emitted by boreal and temperate wildland fires at northern latitudes, J. Geophys. Res., 105, 26871–26890, 2000.

Lehsten, V., Tansey, K., Balzter, H., Thonicke, K., Spessa, A., Weber, U., Smith, B., and Arneth, A.: Estimating carbon emissions from African wildfires, Biogeosciences, 6, 349–360, doi:10.5194/bg-6-349-2009, 2009.

Lobert, J. M. and Warnatz, J.: Emissions from the combustion process in vegetation, in: Fire in the environment: The ecological, atmospheric, and climatic importance of vegetation fires, edited by: Crutzen, P. J. and Goldammer, J. G., Wiley, Chichester, 15–37, 1993.

Mayaux, P., Bartholome, E. M. C., Eva, H. D., Van Custem, C., Cabral, A., Nonguierma, A., Diallo, O., Pretorius, C., Thompson, M., Cherlet, M., Pekel, J.-F., Defourny, P., Vasconcelos, M., Di Gregorio, A., Fritz, S., De Grandi, G., Elvidge, C., Vogt, P., and Belward, A. S.: A Land Cover Map of Africa, Carte de l'Occupation du Sol de l'Afrique, European Commission, JRC24914, 2003.

McMillan, W. W., Barnet, C., Strow, L., Chahine, M. T., McCourt, M. L., Warner, J. X., Novelli, P. C., Korontzi, S., Maddy, E. S., and Datta, S.: Daily global maps of carbon monoxide from NASA's Atmospheric Infrared Sounder, Geophys. Res. Lett., 32, L11801, doi:10.1029/2004GL021821, 2005.

McMillan, W. W., Warner, J. X., McCourt Comer, M., Maddy, E., Chu, A., sparling, L., Eloranta, E., Hoff, R., Sachse, G., Barnet, C., Razenkov, I., and Wolf, W.: AIRS views transport from 12 to 22 July 2004 Alaskan/Canadian fires: Correlation of AIRS CO and MODIS AOD with forward trajectories and comparison of AIRS CO retrievals with DC-8 in situ measurements during INTEX-A/ICARITT, J. Geophys. Res., 113, D20301, doi:10.1029/2007JD009711, 2008.

Pierangelo, C., Chédin, A., Heilliette, S., Jacquinet-Husson, N., and Armante, R.: Dust altitude and infrared optical depth from AIRS, Atmos. Chem. Phys., 4, 1813–1822, doi:10.5194/acp-4-1813-2004, 2004.

Pyne, S. J., Andrews, P. L., and Laven, R. D., Introduction to Wildland Fire, 2nd Edn., John Wiley, New York, 14–25, 1996.

Rio, C., Hourdin, F., and Chédin, A.: Numerical simulation of tropospheric injection of biomass burning products by pyro-thermal plumes, Atmos. Chem. Phys., 10, 3463–3478, doi:10.5194/acp-10-3463-2010, 2010.

Roberts, G., Wooster, M. J., and Lagoudakis, E.: Annual and diurnal african biomass burning temporal dynamics, Biogeosciences, 6, 849–866, doi:10.5194/bg-6-849-2009, 2009.

Roy, D. P., Boschetti, L., Justice, C. O., and Ju, J.: The collection 5 MODIS burnt area product – Global evaluation by comparison with the MODIS active fire product, Remote Sens. Environ., 112, 3690–3707, 2008.

Schultz, M. G., Heil, A., Hoelzemann, J. J., Spessa, A., Thonicke, K., Goldammer, J. G., Held, A. C., Pereira, J. M. C., and van het Bolscher, M.: Global wildland fire emissions from 1960 to 2000, Global Biogeochem. Cy., 22, GB2002, doi:10.1029/2007GB003031, 2008.

Scott, N. A. and Chédin, A.: A fast line-by-line method for atmospheric absorption computations: The Automatized Atmospheric Absorption Atlas, J. Appl. Meteorol., 20, 802–812, 1981.

Seiler, W. and Crutzen, P. J.: Estimates of gross and net fluxes of carbon between the biosphere from biomass burning, Climatic Change, 2, 207–247, 1980.

Spivakovsky, C. M., Yevich, R., Logan, J. A., Wofsy, S. C., McElroy, M. B., and Prather, M. J.: Tropospheric OH in a three-dimensional chemical tracer model: An assessment based on observations of CH_3CCl_3, J. Geophys. Res., 95, 18441–18471, 1990.

Streets, D. G., Zhang, Q., Wang, L., He, K., Hao, J., Wu, Y., Tang, Y., and Carmichael, G. R.: Revisiting China's CO emissions after Transport and Chemical Evolution over the Pacific (TRACE-P) mission: Synthesis of inventories, atmospheric modeling, and observations, J. Geophys. Res., 111, D14306, doi:10.1029/2006JD007118, 2006.

Thonat, T., Crevoisier, C., Scott, N. A., Chédin, A., Schuck, T., Armante, R., and Crépeau, L.: Retrieval of tropospheric CO column from hyperspectral infrared sounders – application to four years of Aqua/AIRS and MetOp-A/IASI, Atmos. Meas. Tech., 5, 2413–2429, doi:10.5194/amt-5-2413-2012, 2012.

Turquety, S., Logan, J. A., Jacob, D. J., Hudman, R. C., Leung, F. Y., Heald, C. L., Yantosca, R. M., Wu, S., Emmons, L. K., Edwards, D. P., and Sachse, G. W.: Inventory of boreal fire emissions for North America in 2004: Importance of peat burning and pyroconvective injection, J. Geophys. Res., 112, D12S03, doi:10.1029/2006JD007281, 2007.

Turquety, S., Hurtmans, D., Hadji-Lazaro, J., Coheur, P.-F., Clerbaux, C., Josset, D., and Tsamalis, C.: Tracking the emission and transport of pollution from wildfires using the IASI CO retrievals: analysis of the summer 2007 Greek fires, Atmos. Chem. Phys., 9, 4897–4913, doi:10.5194/acp-9-4897-2009, 2009.

van der Werf, G. R., Randerson, J. T., Giglio, L., Collatz, G. J., Kasibhatla, P. S., and Arellano Jr., A. F.: Interannual variability in global biomass burning emissions from 1997 to 2004, Atmos. Chem. Phys., 6, 3423–3441, doi:10.5194/acp-6-3423-2006, 2006.

van der Werf, G. R., Randerson, J. T., Giglio, L., Collatz, G. J., Mu, M., Kasibhatla, P. S., Morton, D. C., DeFries, R. S., Jin, Y., and van Leeuwen, T. T.: Global fire emissions and the contribution of deforestation, savanna, forest, agricultural, and peat fires (1997–2009), Atmos. Chem. Phys., 10, 11707–11735, doi:10.5194/acp-10-11707-2010, 2010.

Ward, D. E., Hao, W. M., Susott, R. A., Babitt, R. E., Shea, R. W., Kauffman, J. B., and Justice, C. O.: Effect of fuel composition efficiency and emission factors for African savanna ecosystems, J. Geophys. Res., 101, 23569–23576, 1996.

Wooster, M. J., Roberts, G., Perry, G. L. W., and Kaufman, Y. J.: Retrieval of biomass combustion rates and totals from fire radiative power observations: FRP derived and calibration relationships between biomass consumption and fire radiative energy release, J. Geophys. Res., 110, D24311, di:10.1029/2005JD006318, 2005.

Yurganov, N. L., McMillan, W. W., Dzhola, A. V., Grechko, E. I., Jones, N. B., and van der Werf, G. R.: Global AIRS and MOPITT CO measurements: Validation, comparison, and links to biomass burning variations and carbon cycle, J. Geophys. Res., 113, D09301, doi:10.1029/2007JD009229, 2008.

Yurganov, L. N., Rakitin, V., Dzhola, A., August, T., Fokeeva, E., George, M., Gorchakov, G., Grechko, E., Hannon, S., Karpov, A., Ott, L., Semutnikova, E., Shumsky, R., and Strow, L.: Satellite- and ground-based CO total column observations over 2010 Russian fires: accuracy of top-down estimates based on thermal IR satellite data, Atmos. Chem. Phys., 11, 7925–7942, doi:10.5194/acp-11-7925-2011, 2011.